JOURNAL OF Materials CHEMISTRY

Gas-phase formation of zinc/cadmium chalcogenide cluster complexes and their solid-state thermal decomposition to form II–VI nanoparticulate material

Nigel L. Pickett,[a]† Steven Lawson,[a] W. Gregor Thomas,[a] Frank G. Riddell,[a] Douglas F. Foster,[a] David J. Cole-Hamilton* and John R. Fryer[b]

[a] *School of Chemistry, The University of St. Andrews, St. Andrews, Fife, UK KY16 9ST. E-mail: djc@st-and.ac.uk*
[b] *Department of Chemistry, Glasgow University, Glasgow, UK G12 8QQ*

Received 14th August 1998, Accepted 30th September 1998

Gas-phase reactions between R_2Zn (R = Me and Et) and ^tBuSH produce cluster complexes of the type $[RZnS^tBu]_n$. These clusters, along with $[MeZnS^tBu(py)]_2$ (py = pyridine), have been characterised by $^{13}C\{^1H\}$ solid-state NMR. On heating to 100 °C in the solid-state, the complexes $[MeZnS^tBu]_5$ and $[MeZnS^tBu(py)]_2$ release dimethylzinc (Me_2Zn) to form the zinc *bis*(thiolate) compound, $[Zn(S^tBu)_2]_n$, with further heating (>200 °C) leading to the formation of ZnS. The ethyl analogue, $[EtZnS^tBu]_5$, does not lose Et_2Zn on heating and thermogravimetric analysis (TGA) suggests a different decomposition pathway, one which mainly involves loss of the organic moieties without the concurrent loss of volatile Zn or S compounds, although ZnS is again the final thermal decomposition product. The decomposition of the involatile pentamers, $[MeZnS^tBu]_5$ and $[EtZnS^tBu]_5$, and the dimer, $[MeZnS^tBu(py)]_2$, proceeds at higher temperature (200–350 °C) to give agglomerates of ME nanoparticulate material, with the individual particles having diameters of 2–20 nm in all cases. The mechanistic pathway by which these clusters decompose appears to be highly dependent upon the R group (Me or Et) present within the cluster. Preliminary results suggest that complexes of the type $[RME^tBu]_n$ are also produced from the gas-phase reactions of Me_2Zn with ^tBuSeH and from Me_2Cd with ^tBuSH.

Introduction

The use of metal organic vapour phase epitaxy (MOVPE) to produce single-crystal layers of wide band gap 12–16 (II–VI) materials (ZnS, ZnSe, CdS and CdSe) is now an established technique. The most common method still employs the thermally controlled reaction between a group 12 dialkyl compound, R_2M (R = Me, Et *etc.*; M = Zn and Cd) and a group 16 hydride (H_2S or H_2Se).[1] However, a premature reaction (prereaction) which takes place between the two precursors in the cold zone of the growth cell, upstream of the heated substrate, can cause adverse effects on the properties of the grown epilayers. It has been shown that the introduction of a σ-donor compound to the reaction system can lead to a dramatic reduction of the prereaction. Compounds which have been investigated as prereaction suppressants include: 1,4-dioxane,[2–4] thioxane,[4] triethylamine,[5,6] 1,3,5-trimethylhexahydro-1,3,5-triazine,[6] *N*,*N*,*N*′,*N*′-tetramethylethane-1,2-diamine,[7] *N*,*N*,*N*′,*N*′-tetramethyldiaminomethane[8] and pyridine.[9]

While investigating the nature of the prereaction, recent studies of ours[10] have shown that the gas-phase reactions that occur between H_2S/H_2Se and Me_2Cd/Me_2Zn result in the formation of chalcogenide deposits (ZnS, ZnSe, CdS and CdSe), with the deposits consisting of poorly formed nanocrystalline material of the hexagonal phase within the size range 10–100 nm. The addition of small amounts of pyridine to the reaction system greatly improves the crystallinity exhibited by the particles, while addition of larger quantities of pyridine retains the improved crystal quality whilst also leading to a decrease in particle size. The ability of pyridine to influence the particle size decreases in the order ZnS > CdS > CdSe > ZnSe. These results, along with the work of others,[11] allowed us to propose a mechanism by which particle nucleation, growth, and suppression of growth by pyridine can be explained.[10c]

In the absence of a Lewis base (pyridine), particle growth occurs by initial association between R_2M and H_2E leading to the formation of $[RMEH]_2$, which grows rapidly into clusters of the type, $HE_n(ME)_xMR_m$, consisting of a central ME core with E–H and M–R fragments on the surface of the particles, which are suspended within the carrier-gas. Surface bound M–R fragments react with gas-phase H_2E leading to the elimination of RH and formation of new E–H surface bound fragments. These E–H sites in turn react with gas-phase R_2M leading to the formation of new M–R sites on the continuously growing particles. Termination of particle growth may occur by pyridine binding to the reactive surface M–R sites, preventing their reaction with H_2E by a blocking mechanism.[10c]

One step of this growth mechanism involves the reaction of surface bound E–H fragments with R_2M to eliminate RH. Thus, one other approach that can be used in an effort to eliminate prereactions in the growth of II–VI semiconductors is to reduce or eliminate E–H bonds in the group 16 precursors. A number of research groups have, in their efforts to control II–VI epitaxial growth, used a range of dialkyl sulfides/selenides and thiols/selenols as the group 16 precursor. The most promising alternative group 16 precursors are those which are bound to *tert*-butyl groups *i.e.* $^tBu_2S$[12] and $^tBu_2Se$,[13] along with ^tBuSH[14,15] and ^tBuSeH.[16]

Although successful II–VI growth has been achieved with ^tBuSH in combination with Me_2Zn, Et_2Zn and Me_2Cd,[14,15] it has been suggested that the prereaction is only totally eliminated when Et_3N is added to the growth system.[17] Herein, we report that in the gas-phase ^tBuEH and R_2M (R = Et, Me; M = Zn, Cd; E = S, Se) react to form zinc/cadmium chalcogenide cluster complexes of the type $[RME^tBu]_n$. The formation, characterisation and solid-state thermal decomposition of these

†Current address: School of Chemistry and Biochemistry, and School of Materials Science and Engineering and Molecular Design Institute, Georgia Institute of Technology, Atlanta, Georgia 30332–0400, USA.

clusters is described and discussed, with the goal of advancing the understanding of the epitaxial growth process using both conventional and single-source precursors.[18]

Experimental

General

Microanalytical data were obtained at the University of St. Andrews. Analysis of samples by powder X-ray diffraction (PXRD) were carried out on a Stöe STADI/P diffractometer using Cu-Kα radiation with data collected in the transmission mode. Transmission electron micrographs (TEM) were obtained at the University of St. Andrews on a Phillips EM 301 microscope at 80 keV and at Glasgow University on a JEOL 1200 EX operated at 120 keV (point resolution of 0.3 nm) or on a ABT 002B operated at 200 keV (point resolution of 0.18 nm). Particle sizes were determined by direct measurement of individual particles from the transmission electron micrographs. $^{13}C\{^1H\}$ solid-state NMR spectra were obtained on a Brüker MSL 500 spectrometer using CPMAS accumulation techniques with chemical shifts referenced to the CH_2 resonance (δ 38.56) of an external adamantane sample. Solution NMR data were recorded on a Brüker Associates AM300 spectrometer operating in the Fourier transform mode with (for ^{13}C) noise proton decoupling. The $^{13}C\{^1H\}$ and ^1H NMR spectra were run in deuteriated solvents for the lock signal, as given for each spectrum, with chemical shifts in ppm to high frequency of tetramethylsilane (TMS) as the internal reference. The ^2H NMR spectra were run in non-deuteriated solvent, as given for each spectrum, with a few drops of the deuteriated analogue to act as both the lock signal and internal reference—the ^2H NMR signals were then back-referenced to TMS by using the known shift of the solvent relative to TMS. Simultaneous thermal analyses [STA, thermogravimetric analysis—differential temperature analysis (TGA–DTA)] were performed on a 'TA Instruments SDT 2960 Simultaneous DTA-TGA' instrument.

Dry oxygen free nitrogen, helium and argon (BOC), purified by passing through two consecutive columns (2.5 $\times$ 80 cm) packed with Cr^{2+} on silica, were used as the carrier gases and as the inert atmospheres under which all preparations and manipulations were carried out. Greaseless joints and taps were employed and manipulations were carried out using standard Schlenk line and catheter tubing techniques. Dimethylcadmium, dimethylzinc and diethylzinc were prepared and purified as described previously.[19] $ZnCl_2$, Mg turnings, ^{t}BuMgCl (2.0 mol dm^{-3} in Et_2O), C_2D_5OH, pyridine and ^{t}BuSH were purchased from Aldrich and the pyridine and ^{t}BuSH distilled from CaH_2 prior to use. Amorphous Se powder (mesh size $<$325) was purchased from Johnson Matthey. C_2D_5OH was transformed into C_2D_5Br by a standard method on treatment with HBr. Light petroleum (bp 40–60 °C) and diethyl ether were dried by distillation from sodium diphenylketyl and degassed prior to use.

Preparation of precursors

^{t}BuSeH. A standard solution of ^{t}BuMgCl in Et_2O (250 cm^3, 2.0 mol dm^{-3}, 0.5 mol) was further diluted by the addition of 750 cm^3 Et_2O. Selenium powder (39.5 g, 0.50 mol) was added in small batches over 2 h to the rapidly stirred Grignard solution to form a voluminous white precipitate of ^{t}BuSeMgCl. The suspension was stirred overnight before being cooled in an ice bath and hydrolysed by the cautious addition of aqueous HCl (600 cm^3, 1 mol dm^{-3}, 0.6 mol). The clear pale-yellow organic layer was separated and the lower colourless aqueous layer extracted with 3 $\times$ 100 cm^3 of Et_2O. The combined organic extracts were dried over $MgSO_4$ followed by CaH_2. Finally, the ^{t}BuSeH, a clear, colourless and slightly light sensitive liquid, was separated from Et_2O and purified by fractional distillation at normal pressure through a high efficiency (30 theoretical plates) Spaltrohr® (Fisher Scientific UK) distillation column. Bp 79–80 °C. Yield after purification 48 g (70%). $^{13}C\{^1H\}$ NMR (C_6D_6), δ 36.06 (s, SeC(CH_3)$_3$) and 38.77 (s, Se*C*). ^1H NMR (C_6D_6), δ 0.10 (s, 1H, Se*H*) and 1.40 [s, 9H, SeC(CH_3)$_3$].

$(C_2D_5)_2Zn$. A Grignard solution of CD_3CD_2MgBr in 100 cm^3 of Et_2O was prepared from 23 g of CD_3CD_2Br (0.20 mol) and 6 g of Mg turnings (0.25 mol). This Grignard solution was added dropwise to a rapidly stirred solution of 13.0 g of $ZnCl_2$ (0.095 mol) in 100 cm^3 of Et_2O at a rate sufficient to maintain a steady reflux (*ca.* 30 min). The resulting suspension was externally heated to reflux for 1 h after complete addition of the Grignard reagent. All volatiles were collected by trap-trap distillation *in vacuo* into a -196 °C cold trap and the $(C_2D_5)_2Zn$ subsequently purified by fractional distillation. Bp 118 °C. Yield 11.4 g, 90%. $^{13}C\{^1H\}$ NMR (C_6D_6), δ 5.74 (qnt, J_{D-C} = 18.5 Hz, Zn*C*D_2CD$_3$), 9.24 (spt, J_{D-C} = 19.0 Hz, ZnCD$_2$*C*D$_3$). ^2H NMR (C_6H_6–C_6D_6), δ 0.27 (br s, 2 ^2H, Zn*C*D_2CD$_3$), 1.20 (br s, 3 ^2H, ZnCD$_2$*C*D$_3$).

[MeZnS^{t}Bu]$_5$. This compound was prepared according to the literature procedure,[20] from the low temperature (-78 °C) reaction between Me_2Zn and ^{t}BuSH in light petroleum. Yielding, after work-up, a white powder of the product. Found: C, 35.29; H, 7.65; $C_{25}H_{60}S_5Zn_5$ requires C, 35.41; H, 7.13%. Solid-state $^{13}C\{^1H\}$ NMR, δ -8.20 (s, Zn*C*H$_3$), -6.76 (s, Zn*C*H$_3$), -5.78 (s, 2Zn*C*H$_3$), -0.84 (s, Zn*C*H$_3$), 35.39 [s, SC(*C*H$_3$)$_3$], 36.09 [s, SC(*C*H$_3$)$_3$], 36.43 [s, SC(*C*H$_3$)$_3$], 36.50 [s, SC(*C*H$_3$)$_3$], 36.80 [s, SC(*C*H$_3$)$_3$], 46.64 (s, S*C*), 50.83 (s, S*C*), 51.59 (s, S*C*), 52.45 (s, S*C*), 52.74 (s, S*C*).

[MeZnS^{t}Bu(py)]$_2$. This compound was prepared according to the literature procedure,[20] from the low temperature (-78 °C) reaction between Me_2Zn, ^{t}BuSH and pyridine in light petroleum. Yielding, after work-up, a white powder of the product. Found: C, 47.84; H, 6.83; N, 4.99; $C_{20}H_{34}S_2N_2Zn_2$ requires C, 48.30; H, 6.89; N, 5.63%. Solid-state $^{13}C\{^1H\}$ NMR, δ -7.29 (s, 2Zn*C*H$_3$), 36.77 [s, SC(*C*H$_3$)$_3$], 37.92 [s, SC(*C*H$_3$)$_3$], 43.42 (s, S*C*), 43.91 (s, S*C*), 124.14 (s, py*C*), 124.91 (s, py*C*), 138.69 (s, py*C*), 149.64 (br s, 2py*C*).

Gas-phase preparation of Zn and Cd chalcogenide cluster complexes

Prereaction experiments were conducted at just above atmospheric pressure (101.350 Pa) using an experimental set-up as schematically illustrated in Fig. 1. Carrier-gas containing specific gas-phase concentrations of reactants [Me_2Cd, Me_2Zn, Et_2Zn and $(C_2D_5)_2Zn$ together with ^{t}BuSeH or ^{t}BuSH] were allowed to meet at the same point along a horizontal quartz tube. Total gas flow through the apparatus was in the range 300–450 cm^3 min^{-1} and the gas-phase concentration of individual reactants in the range 1×10^{-3}–1×10^{-2} mol dm^{-3}. Effluent gases containing unused reactants and any volatile products were allowed to pass through neutralising solutions followed by an industrial scrubber before being released into a fumehood. For specific experiments, effluent gas containing any volatile products was diverted *via* a gas sampling port to a gas chromatograph (HP 5890)—mass spectrometer (HP 5972 series mass selective detector) for analysis (GC-MS).

[EtZnS^{t}Bu]$_5$. Using the experimental set-up as described above, the gas-phase mixing of stoichiometric quantities of Et_2Zn and ^{t}BuSH produced a fine white powder along the entire length of the quartz tube. Attempts to obtain a satisfactory elemental analysis were hampered by the sample constantly losing weight when exposed to air owing to hydrolysis. Solid-state $^{13}C\{^1H\}$ NMR, δ 5.85 (s, Zn*C*H$_2$CH$_3$), 6.30

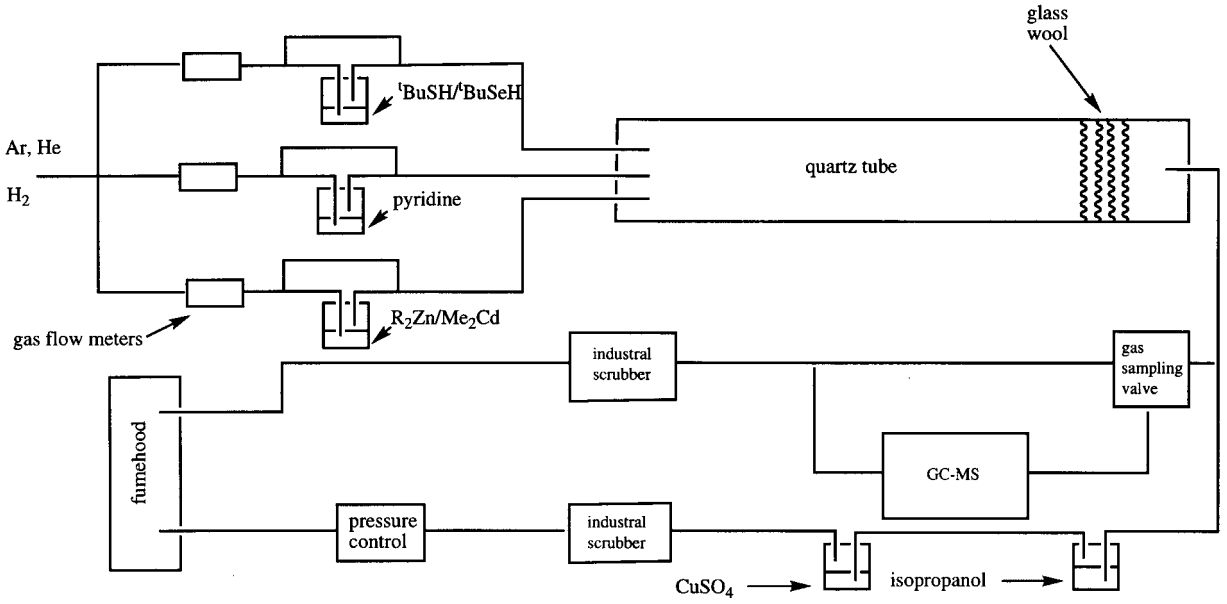

Fig. 1 Schematic diagram of the experimental set-up used both in the preparation and solid-state thermolysis of metal chalcogenides cluster complexes.

(s, $ZnCH_2CH_3$), 7.19 (s, $ZnCH_2CH_3$), 7.69 (s, $ZnCH_2CH_3$), 8.63 (s, $ZnCH_2CH_3$), 14.13 (s, $ZnCH_2CH_3$), 14.61 (br s, $2ZnCH_2CH_3$), 14.77 (br s, $2ZnCH_2CH_3$), 35.94 [s, $SC(CH_3)_3$], 36.21 [s, $SC(CH_3)_3$], 36.43 [s, $SC(CH_3)_3$], 36.75 [s, $SC(CH_3)_3$], 36.92 [s, $SC(CH_3)_3$], 45.47 (s, S*C*), 50.18 (s, S*C*), 50.46 (s, S*C*), 50.93 (s, S*C*), 51.34 (s, S*C*).

[MeZnSe^{t}Bu]$_n$. The gas-phase mixing of stoichiometric quantities of Me_2Zn and ^{t}BuSeH produced a white deposit. Attempts to obtain a satisfactory elemental analysis were again hampered by the sample constantly losing weight when exposed to air owing to hydrolysis. The solid-state $^{13}C\{^1H\}$ NMR spectrum consisted of broad peaks which merged into one another, but which had a similar appearance to those of [MeZnS^{t}Bu]$_5$. ^{1}H NMR (CD_2Cl_2), δ −0.40 (s, $ZnCH_3$), 1.70 [s, $SC(CH_3)_3$].

[MeCdS^{t}Bu]$_n$. The gas-phase mixing of stoichiometric quantities of Me_2Cd and ^{t}BuSH produced a white deposit. The solid-state $^{13}C\{^1H\}$ NMR again gave broad peaks which merged into one another, but which had a similar appearance to those of [MeZnS^{t}Bu]$_5$. Solid-state $^{13}C\{^1H\}$ NMR, δ −9.53 (br, $CdCH_3$), −5.81 (br, $CdCH_3$), 37.44–39.31 [br, $SC(CH_3)_3$], 48.96–50.29 (br, S*C*).

Solid-state thermal decomposition of Zn chalcogenide cluster complexes

A similar experimental set-up to that used above in the preparation and collection of prereaction deposits was employed (Fig. 1), with known amounts of metal chalcogenide cluster complexes contained inside a ceramic crucible placed inside the quartz tube and at the centre of the furnace. A carrier gas (Ar), at just above atmospheric pressure (101.350 Pa), was passed along the quartz tube at a flow rate of 200 cm^3 min^{-1} while the furnace was heated to a maximum temperature of 600 °C. As in the case of the preparation of prereaction deposits, effluent gas containing unused reactants and any volatile products was allowed to pass through neutralising solutions followed by an industrial scrubber before being released into a fumehood. For specific experiments, effluent gas containing any volatile products was diverted *via* a gas sampling port to the GC-MS.

[MeZnS^{t}Bu]$_5$: weight before thermolysis, 0.52 g; weight of residue, 0.16 g; 69.2% weight loss. [MeZnS^{t}Bu(py)]$_2$: weight before thermolysis, 1.53 g; weight of residue, 0.32 g; 79.1% weight loss. [EtZnS^{t}Bu]$_5$: weight before thermolysis, 3.15 g; weight of residue, 1.45 g; 54.0% weight loss.

Formation of [Zn(S^{t}Bu)$_2$]$_n$ from [MeZnS^{t}Bu(py)]$_2$

Heating [MeZnS^{t}Bu(py)]$_2$ to 100 °C *in vacuo* (*ca.* 1 h) liberated a colourless liquid, which was collected in a cold trap. This left a dirty white solid. The colourless liquid distillate was shown to be [$Me_2Zn(py)_2$]: ^{1}H NMR, δ −0.70 (s, $ZnCH_3$), 7.32 (m, py*H*), 7.72 (m, py*H*), 8.58 (m, py*H*). $^{13}C\{^1H\}$ NMR, δ −12.34 (s, $ZnCH_3$), 124.07 (m, py*C*), 136.69 (m, py*C*), 149.44 (m, py*C*). The white solid was identified as impure [Zn(S^{t}Bu)$_2$]$_n$: Found: C, 37.55; H, 7.47; N, 0.24; $C_8H_{18}S_2Zn$ requires C, 39.41; H, 7.44%. Solid-state $^{13}C\{^1H\}$ NMR, δ 36.96 [s, $SC(CH_3)_3$], 49.20 (s, S*C*), 50.08 (s, S*C*).

Results and discussion

Synthesis and characterisation of Zn and Cd chalcogenide cluster complexes

Using the system described in the experimental section, the gas-phase mixing at room temperature of stoichiometric amounts of Et_2Zn and ^{t}BuSH (He carrier gas) resulted in the formation of a fine white powder deposit. GC-MS analysis of the effluent carrier-gas confirmed that ethane is the only gaseous by-product of this reaction. When Et_2Zn was replaced by the deuteriated analogue, $(C_2D_5)_2Zn$, the ethane produced was pure C_2D_5H, formed by protonation of $(C_2D_5)_2Zn$ by the acidic S–H of ^{t}BuSH. Upon exposure to air, the white powder gave off a strong smell of thiol, presumably due to hydrolysis rather than from any remaining ^{t}BuSH. Without further purification, solid-state $^{13}C\{^1H\}$ NMR analysis of the powder gave a spectrum [Fig. 2(a)] which exhibits five different sets of ethyl resonances along with five different ^{t}Bu resonances. These results confirmed the presence of at least five different environments for both Zn and S within the deposit and the probable identity of the complex as the thiolate pentamer, [EtZnS^{t}Bu]$_5$. A non-quaternary $^{13}C\{^1H\}$ suppression spectrum (which greatly reduces the intensity of *C*H and *C*H$_2$ resonances) [Fig. 2(b)] shows the methyl signals of the ethyl groups, $ZnCH_2CH_3$, to be down field of the methylene, $ZnCH_2CH_3$, signals due to the shielding effect of the zinc. Attempts to establish the structure of the complex by X-ray

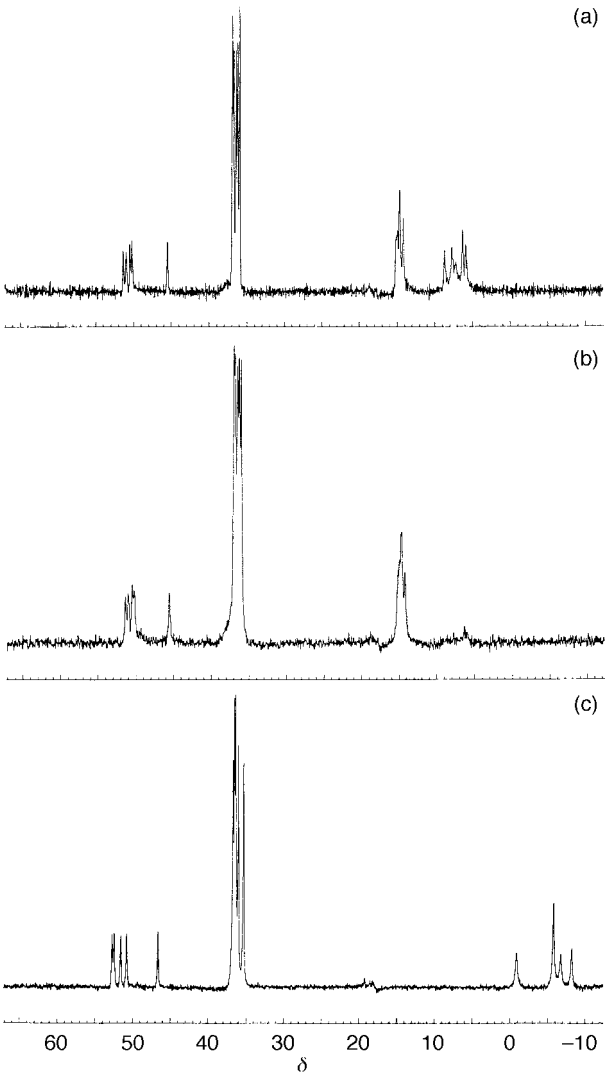

Fig. 2 Solid-state $^{13}C\{^1H\}$ NMR spectra of (a) $[EtZnS^tBu]_5$, (b) non-quaternary suppression spectrum of $[EtZnS^tBu]_5$ and (c) $[MeZnS^tBu]_5$.

crystallography were thwarted due to our inability to grow X-ray quality crystals. However, the solid-state $^{13}C\{^1H\}$ NMR data of the ethyl complex suggested the complex to be isostructural with the methyl pentamer, $[MeZnS^tBu]_5$, first synthesised by Coates and Ridley,[20] and more recently structurally characterised by O'Brien and coworkers.[11] Thus, in an attempt to confirm the likely structure of the ethyl complex $[EtZnS^tBu]_5$, $[MeZnS^tBu]_5$ was prepared by the literature method[20] and characterised by solid-state $^{13}C\{^1H\}$ NMR spectroscopy.

The solid-state $^{13}C\{^1H\}$ NMR spectrum of $[MeZnS^tBu]_5$ does indeed correlate well with that of the ethyl complex, essentially exhibiting five different ^{t}Bu resonances and four methyl resonances in a 1:2:1:1 ratio [Fig. 2(c)]. Interestingly, $[MeZnS^tBu]_5$ is fluxional in solution (C_6D_6) with the ^1H NMR spectrum exhibiting single resonances for all five $ZnCH_3$ groups and for all five ^{t}Bu groups while the $^{13}C\{^1H\}$ solution spectrum of $[MeZnS^tBu]_5$ also exhibits only one $ZnCH_3$ resonance and one *tert*-butyl resonance.[11] This fluxionality is quenched in the solid-state, at least up to 25 °C. Thus, the NMR data strongly support the view that in the solid-state $[EtZnS^tBu]_5$ and $[MeZnS^tBu]_5$ are isostructural, as schematically shown in Fig. 3. The structure consists of a cubic arrangement of zinc and sulfur atoms with one edge of the cube broken open by the addition of the extra Zn–S unit, resembling a supermarket trolley. The solid-state $^{13}C\{^1H\}$ NMR data of both the methyl and ethyl complexes (Fig. 2) show the resonance for one of the quaternary carbon atoms

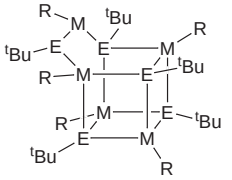

Fig. 3 The basic structure of $[RME^tBu]_5$ (M = Zn, Cd; E = S, Se; R = Me, Et).

of the *tert*-butyl groups to be significantly shifted to higher magnetic field strength relative to the shifts of the other four. This unique resonance probably arises from the *tert*-butyl group in the 'handle' section of the molecule and the shift to higher field is probably due to the sulfur being bonded to two rather than three adjacent zinc atoms (resulting in a higher shielding effect). Similarly, in $[MeZnS^tBu]_5$, one of the $ZnCH_3$ carbon resonances is clearly distinct from the others, with a shift this time to lower field, and again, this is probably the resonance of the $ZnCH_3$ group in the 'handle' section of the molecule, which is deshielded due to the zinc atom being bonded to only two adjacent sulfur atoms rather than three as for all the other zinc atoms.

White powders were also obtained from the gas-phase reactions of Me_2Cd with ^{t}BuSH and from Me_2Zn with ^{t}BuSeH. Although both compounds afford poorly resolved solid-state $^{13}C\{^1H\}$ NMR spectra, the over-all shapes of the spectra are again similar to that of $[MeZnS^tBu]_5$, suggesting that cluster complexes of the type $[MeME^tBu]_n$ are formed. Although the value of n cannot be established from the spectra alone, it has been proposed from NMR data that $n = 4$ for $[MeCdS^tBu]_n$ when prepared from solution.[21,22]

As discussed in the Introduction, for MOVPE growth systems employing R_2M and H_2E (M = Zn, Cd; R = Me, Et; E = S, Se), pyridine can suppress the growth of particulate material by binding to the surface metal atom sites of particles growing within the gas phase. By a similar process, O'Brien and coworkers have reported that the reaction between Me_2Zn, ^{t}BuSH and pyridine in solution (benzene) affords the dinuclear pyridine adduct complex, $[MeZnS^tBu(py)]_2$, rather than the pentamer, $[MeZnS^tBu]_5$, which forms in the absence of pyridine.[11]

These results confirm that for all MOVPE growth systems which involve the gas-phase mixing of thiols/selenols with dialkylzinc/cadmium compounds, a prereaction (detected or otherwise) will occur in the cold zone of the reactor. This will result in the depletion (or complete elimination) of the original precursors from the gas phase before the gas stream carrying the precursors reaches the heated substrate. Moreover, Lovergine *et al.* have reported[17] that the addition of triethylamine to the growth system, when forming ZnS epilayers from ^{t}BuSH and Me_2Zn, although avoiding the formation of solid prereaction deposits, still leads to non-homogeneous epitaxial growth owing to some form of depletion of the two precursors from the gas phase (other than through the epitaxial growth process itself). This observation may be explained by the formation of $[MeZnS^tBu(Et_3N)]_2$ dimers which then either precipitate onto the substrate, or initiate gas-phase particulate growth, with the particulate matter then being precipitated onto the substrate. It is also possible that such dimers are not formed and that Et_3N behaves like pyridine in terminating particulate growth at an early enough stage that prereaction deposits are not visible.[10]

Thermogravimetric analysis and solid-state thermal decomposition of zinc chalcogenide cluster complexes

Because of the current interest in the use of metal chalcogenide complexes as 'single-source' precursors, both in MOVPE growth and nanoparticle material preparation,[18] as well as the

Table 1 Thermal analytical and weight loss data for zinc sulfide cluster complexes

	Step 1[a]			Step 2[a]			Residue (%)[b]		
		Weight loss (%)[b]			Weight loss (%)[b]				
Complex	T_{onset}/ °C	Obs.	Calc.[c]	T_{onset}/ °C	Obs.	Calc.[d]	TGA	Thermolysis	Calc.[e]
$[MeZnS^tBu]_5$	110	24	28	230	45	43	31	31	29
$[MeZnS^tBu(py)]_5$	70	46	51	230	29	29	26	21	20
$[EtZnS^tBu]_5$							48	46	27[f]

[a]From TGA (thermogravimetric analysis). [b]Weight losses and residual weights all relative to initial weight of complex. [c]Loss of half the Zn content as Me_2Zn. [d]Loss of half the S content as $^tBu_2S$. [e]Loss of organics + half the ZnS content. [f]Loss of organics only, gives a calculated residue of 53%.

role that zinc/cadmium chalcogenide cluster complexes might play in MOVPE growth whilst employing separate group 12 and 16 precursors, it is important to understand the thermal properties of complexes of the type: $[EtZnS^tBu]_5$, $[MeZnS^tBu]_5$ and $[MeZnS^tBu(py)]_2$. Simultaneous thermal analyses (STA), thermogravimetric analysis–differential temperature analysis (TGA–DTA) carried out on $[MeZnS^tBu]_5$ and $[MeZnS^tBu(py)]_2$, indicates that these complexes demonstrate similar thermal behaviour [Table 1 and Fig. 4(a) and (b)]. There is a broad endotherm at *ca.* 100 °C with a weight loss corresponding to the loss of all the zinc bound Me groups, as

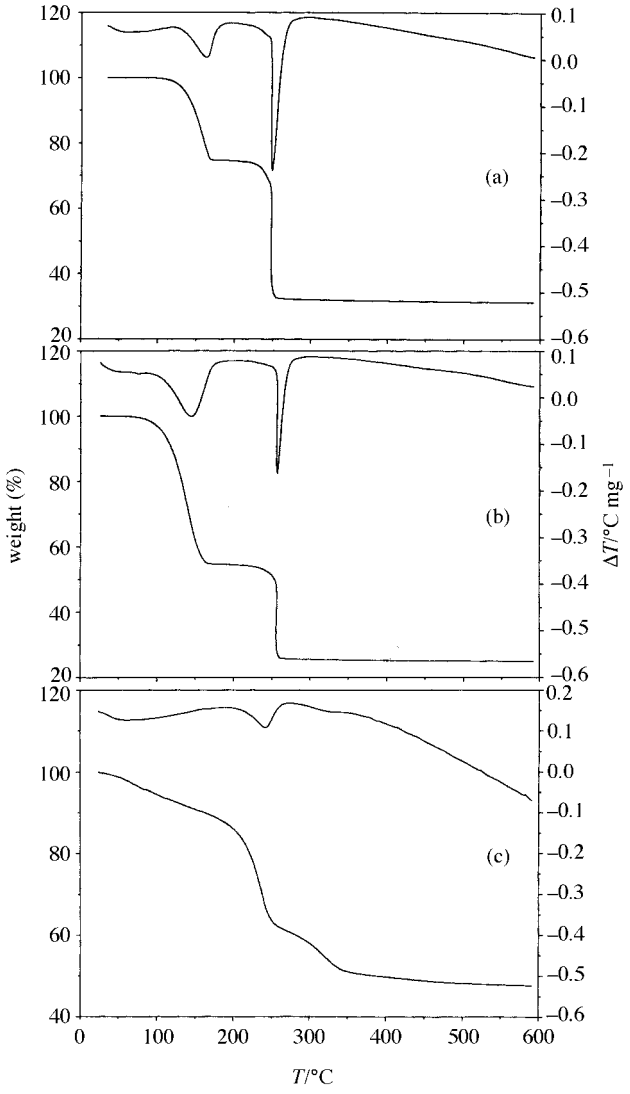

Fig. 4 Simultaneous thermal analyses (STA, thermogravimetric analysis—differential temperature analysis (TGA–DTA)) of (a) $[MeZnS^tBu]_5$, (b) $[MeZnS^tBu(py)]_2$ and (c) $[EtZnS^tBu]_5$.

Me_2Zn or $[Me_2Zn(py)_2]$, and a second sharp endotherm with an onset temperature of *ca.* 230 °C corresponding to the loss of '$^tBu_2S$'. The residue consists of ZnS with a mass corresponding to one half of the total ZnS mass present in the original sample. Macroscopic thermolysis also gave residual weights consistent with this sequence of reactions (Table 1).

GC-MS analysis of the gas-phase products from the macroscopic thermolysis of $[MeZnS^tBu]_5$, under Ar flow, confirmed that Me_2Zn is released but that $^tBu_2S$ is not the only S containing volatile decomposition product, 2-methylpropene and ^{t}BuSH are also produced. Thus, at 100 °C, a trace amount of methane was seen while at 150 °C, traces of methane and 2-methylpropene along with large quantities of Me_2Zn were detected. At 200 °C, large quantities of 2-methylpropene and ^{t}BuSH were detected along with traces of $^tBu_2S$. For the complex $[MeZnS^tBu(py)]_2$, at 100 °C, a large quantity of pyridine was detected along with trace amounts of methane and toluene (resulting from the preparative method), while at 150 °C, pyridine, methane and 2-methylpropene (Me_2Zn was not detected, see below) were observed, and above 200 °C, 2-methylpropene along with trace amounts of $^tBu_2S$ and methane were seen. These results for $[MeZnS^tBu(py)]_2$ do not demonstrate the production of Me_2Zn. We propose that this is due to the presence of pyridine which condenses on the walls of the stainless steel tubing used to connect the thermolysis cell to the gas-sampling valve of the GC-MS. This pyridine will complex with any Me_2Zn released to the gas-phase, forming the solid adduct complex, $[Me_2Zn(py)_2]$. At room temperature, dissociation and revapourisation of $[Me_2Zn(py)_2]$ is at such a slow rate that gas-phase concentrations of Me_2Zn are too low to detect. To confirm that $[MeZnS^tBu(py)]_2$ decomposes by a similar mechanistic pathway to that of $[MeZnS^tBu]_5$, $[MeZnS^tBu(py)]_2$ was heated in the solid state under vacuum to 100 °C. The volatile products were collected in a cold trap and at room temperature gave a viscous liquid, which was shown by ^{1}H NMR to contain Me_2Zn and pyridine. Elemental analysis on the remaining solid, without washing or further purification, suggested it to be the complex $[Zn(S^tBu)_2]_n$. This was confirmed by solid-state $^{13}C\{^1H\}$ NMR as shown in Fig. 5(a). The $^{13}C\{^1H\}$ NMR of the original complex, $[MeZnS^tBu(py)]_2$, is shown in Fig. 5(b) for comparison. The complex, $[Zn(S^tBu)_2)]_n$, shows two peaks of almost equal intensity due to the S*C*^{t}Bu carbons showing that both *syn* and *anti* orientations of the ^{t}Bu groups occur with equal probability. Many complexes of this general formula, $M(ER)_2$, including $[Zn(S^tBu)_2)]_n$,[23f] have previously been prepared and used as potential 'single-source' precursors for II–VI materials.[23] It has been proposed by Steigerwald and Sprinkle that the use of Me_2Cd and R_2Te under MOVPE growth conditions results in the *in situ* formation $Cd(TeR)_2$ which then decomposes to give CdTe.[23h] This could also be occurring in the growth of ZnS from Me_2Zn and ^{t}BuSH.

Although a detailed mechanistic pathway cannot be fully established it appears, from these results, that the overall pathway for the thermal decomposition of $[MeZnS^tBu]_5$ is as

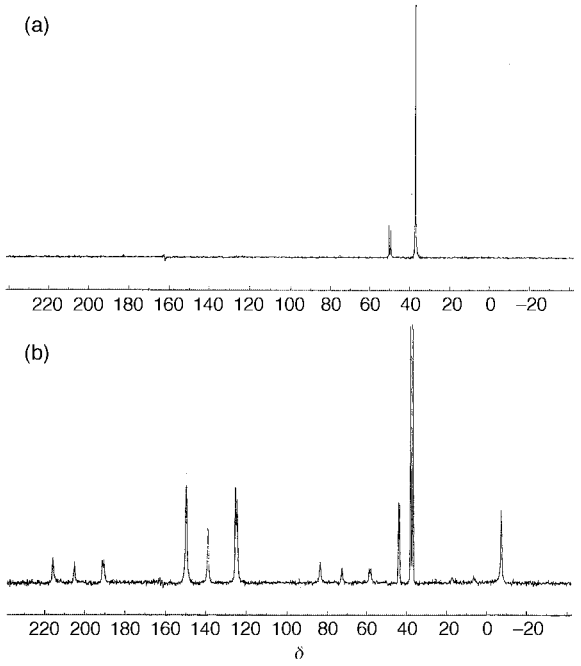

Fig. 5 Solid-state $^{13}C\{^1H\}$ NMR spectra of (a) the residue remaining after heating $[MeZnS^tBu(py)]_2$ to 100 °C and (b) $[MeZnS^tBu(py)]_2$ (the peaks in the range δ 55–85 and δ 190–220 are spinning side bands of the main pyridine resonances at δ 120–155).

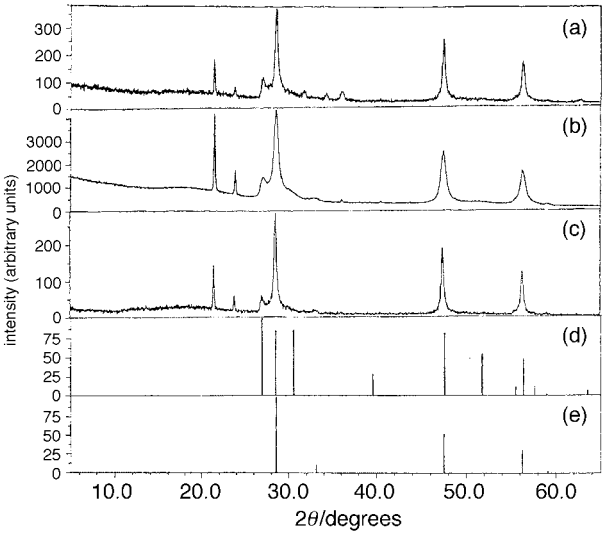

Fig. 6 X-Ray powder diffraction pattern of ZnS formed from the thermolysis of (a) $[EtZnS^tBu]_5$, (b) $[MeZnS^tBu]_5$ and (c) $[MeZnS^tBu(py)]_2$. Standard X-ray powder diffraction patterns of (d) hexagonal (wurtzite) and (e) cubic (sphalerite) phases of ZnS are also shown. The peaks at 2θ 21 and 24° arise from the Vaseline support.

shown in Scheme 1. This involves a rearrangement of the methyl radicals to liberate the volatile compound Me_2Zn, leaving the zinc-*bis*(thiolate), $[Zn(S^tBu)_2]_n$, as a residue. Further heating leads to the loss of *tert*-butyl groups, mainly as 2-methylpropene and ^{t}BuSH along with far smaller amounts of $^tBu_2S$. H_2S might be expected from the decomposition of ^{t}BuSH, but we have shown that the extent of decomposition of ^{t}BuSH is very low below 300 °C.[24] For $[MeZnS^tBu(py)]_2$, a similar process occurs initially to give $[Me_2Zn(py)_2]$ and $[Zn(S^tBu)_2]_n$.

The STA analysis of $[EtZnS^tBu]_5$ is rather different from those of the other compounds, since there is no evidence for formation of $[Zn(S^tBu)_2]_n$ (no sharp exotherm near 230 °C) and the decomposition occurs in three stages [Fig. 4(c)]. The residual mass obtained from both STA and macroscopic thermolysis (*ca.* 47%) is between those expected for the simple loss of the organic moieties (53.1%) and for the type of mechanism described above for $[MeZnS^tBu]_5$ (26.6%). In the thermolysis of $[EtZnS^tBu]_5$, below 100 °C, trace amounts of ethane were detected, at 150 °C, ethane along with larger amounts of 2-methylpropene were seen, while above 200 °C, large amounts of 2-methylpropene along with trace amounts of $^tBu_2S$ were detected. Although trace amounts of compounds containing sulfur were detected, the mechanistic pathway of thermal decomposition involves no major loss of zinc or sulfur. Thus, the decomposition pathway for $[EtZnS^tBu]_5$ is rather different from that for $[MeZnS^tBu]_5$ in that Et_2Zn is not observed as a product, but rather ethane and 2-methylpropene are the major products. One possible decomposition route which explains the volatile product formation involves β-H

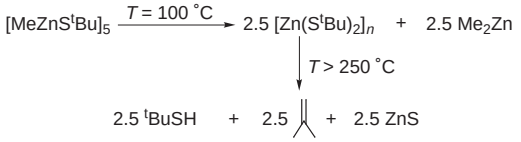

Scheme 1 Schematic representation of the processes occurring in the solid-state thermolysis of $[MeZnS^tBu]_5$.

abstraction from the *tert*-butyl group to form 2-methylpropene and [EtZnSH] with reductive elimination from the latter affording the observed ethane and ZnS. Compounds similar to [EtZnSH] are known to give alkane and ZnS upon thermal decomposition. Why this process should occur for $[EtZnS^tBu]_5$ rather than for $[MeZnS^tBu]_5$ is not clear but demonstrates how a small difference within the precursor can radically alter the pathway by which decomposition takes place.

Analysis of the solid thermolysis residues

The macroscopic thermolysis experiments described above produced grey or white residues, which were scraped from the pyrolysis tube and handled in air before being analysed by powder X-ray diffraction (PXRD) and transmission electron microscopy (TEM). PXRD analyses of all the residues show broad peaks (Fig. 6) and although on first inspection the diffraction patterns appear to resemble the PXRD of cubic (sphalerite) ZnS, previous studies of ours[10,25] along with the calculations of others[26] suggest the residues are more likely to consist mainly of nanoparticles (responsible for the line broadening) of distorted hexagonal (wurtzite) phase ZnS (having a high number of stacking faults and leading to peak dependent line broadening). However, the observation of a peak at $2\theta =$ 33° does suggest that some cubic phase is also present. The diffraction pattern of the residue from $[MeZnS^tBu]_5$ [Fig. 6(b)] is somewhat broader than the others suggesting that the average particle size is smaller.

TEM images for the residue obtained from $[EtZnS^tBu]_5$ [Fig. 7(a)] show the ZnS to be in the form of circular agglomerates 0.5–2 μm in diameter made up of individual ZnS nanoparticles in the size range of 5−10 nm, whilst those from $[MeZnS^tBu]_5$ appear as laths [Fig. 7(b)], which probably arise as a function of sample preparation. Individual crystals within the aggregates are in the size range 5–20 nm. Although high resolution TEM images of the residue formed from $[MeZnS^tBu]_5$ [Fig. 7(c)] reveal many of the nanocrystals to be twinned (or to be composed of a number of subcrystals), there are also a number of perfect single crystals within the residue.

The particles produced on thermolysis by all three complexes are somewhat different from those formed during gas-phase reactions between R_2M and H_2S (M = Zn, Cd) where in general, and especially upon the addition of pyridine, more homogeneous nanoparticles are formed.[10] The particles

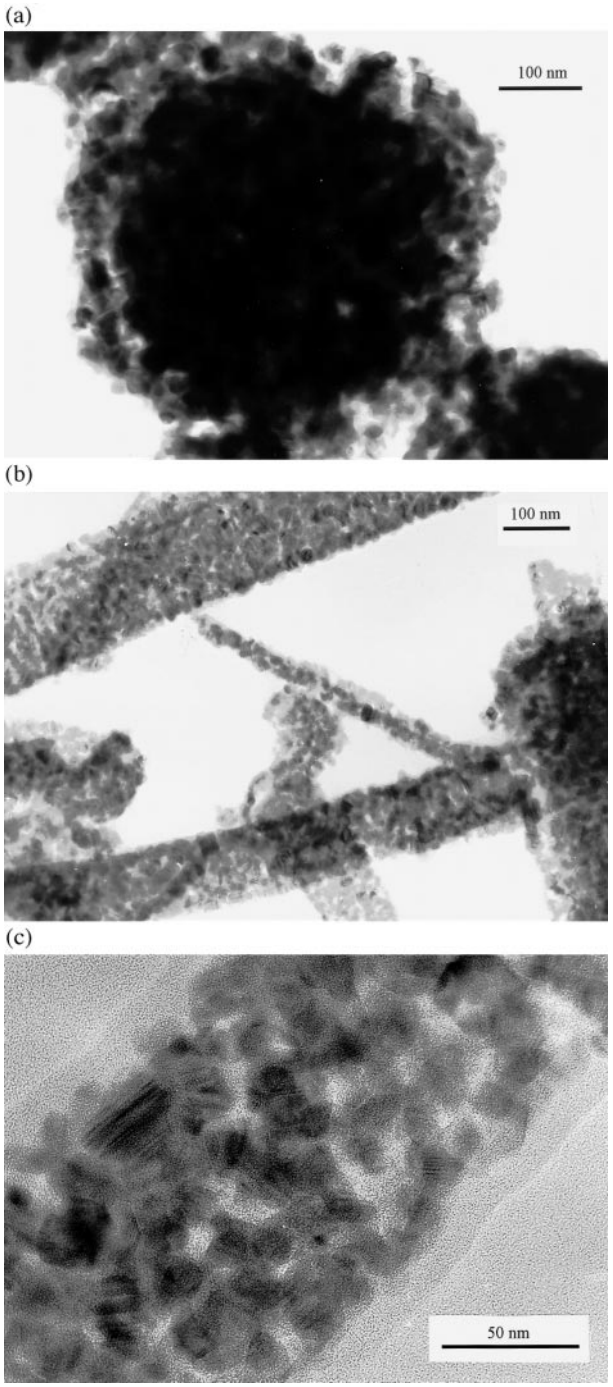

Fig. 7 TEM images of (a) ZnS from the thermolysis of $[EtZnS^tBu]_5$, (b) ZnS from the thermolysis of $[MeZnS^tBu]_5$ and (c) as (b) but at higher magnification.

produced from these chalcogenide cluster complexes are similar to, but larger than, those reported by Steigerwald and coworkers from the solid-state thermolysis of $Zn(SPh)_2$ and $[Zn(SPh)_2(depe)]$ [depe = 1,2-bis(diethylphosphino)ethane].[23i]

Conclusion

Gas-phase mixing of thiols/selenols (REH) with dialkylzinc/cadmium compounds (R_2M) results in the precipitation of zinc/cadmium chalcogenide cluster complexes of general formula $[^tBuEMR]_n$. This demonstrates the importance of avoiding the low temperature premixing of such precursor combinations in the growth of II–VI materials by MOVPE, as this can lead to gas-phase depletion of precursors and non-uniformity in the epitaxial growth. Under the reaction conditions used, the decomposition of the involatile chalcogenide cluster complexes proceeds at higher temperatures (>200 °C) to give agglomerates of nanometer sized particles of metal chalcogenides. However, the pathway by which decomposition occurs seems to be highly dependent upon the alkyl group within the chalcogenide cluster complex.

Acknowledgements

We thank the EPSRC for financial support (N.L.P., *via* a ROPA award, S.L. and D.F.F.) and Ciba Specialty Chemicals for a studentship (W.G.T.).

References

1 (*a*) S. Fujiita, Y. Matsuda and A. Sasaki, *J. Cryst. Growth*, 1984, **68**, 231; (*b*) A. Yoshikawa, S. Muto, S. Yamaga and H. Kasai, *J. Cryst. Growth*, 1988, **86**, 279; (*c*) S. Yamaga, A. Yoshikawa and H. Kasai, *J. Cryst. Growth*, 1988, **86**, 252.
2 P. J. Wright, B. Cockayne, A. J. Williams, A. C. Jones and E. D. Orrell, *J. Cryst. Growth*, 1987, **84**, 552.
3 M. J. Almond, M. P. Beer, M. G. B. Drew and D. A. Rice, *J. Organomet. Chem.*, 1991, **421**, 129.
4 B. Cockayne, P. J. Wright, A. J. Armstrong, A. C. Jones and E. D. Orrell, *J. Cryst. Growth*, 1988, **91**, 57.
5 P. J. Wright, P. J. Parbrook, B. Cockayne, A. C. Jones, E. D. Orrell, K. P. O'Donnell and B. Henderson, *J. Cryst. Growth*, 1989, **94**, 441.
6 P. J. Wright, B. Cockayne, P. J. Parbrook, A. C. Jones, P. O'Brien and J. R. Walsh, *J. Cryst. Growth*, 1990, **104**, 601.
7 M. J. Almond, M. P. Beer, K. Hagen, D. A. Rice and P. J. Wright, *J. Mater. Chem.*, 1991, **1**, 1065.
8 O. Briot, M. DiBlasio, T. Cloitre, N. Briot, P. Bigenwald, B. Gil, M. Averous, R. L. Aulombard, L. M. Smith, S. A. Rushworth and A. C. Jones, *Mater. Res. Soc. Symp. Proc.*, 1994, **340**, 515.
9 P. J. Wright, B. Cockayne, P. J. Parbrook, P. E. Oliver and A. C. Jones, *J. Cryst. Growth*, 1991, **108**, 525.
10 (*a*) N. L. Pickett, D. F. Foster and D. J. Cole-Hamilton, *J. Mater. Chem.*, 1996, **6**, 507; (*b*) N. L. Pickett, D. F. Foster and D. J. Cole-Hamilton, *J. Cryst. Growth*, 1997, **170**, 476; (*c*) N. L. Pickett, F. G. Riddell, D. F. Foster, D. J. Cole-Hamilton and J. R. Fryer, *J. Mater. Chem.*, 1997, **7**, 1855.
11 M. A. Malik, M. Motevalli, J. R. Walsh, P. O'Brien and A. C. Jones, *J. Mater. Chem.*, 1995, **5**, 731.
12 T. Obinata, K. Uesugi, G. Sato, I. Suemune, H. Machida and N. Shimoyama, *Jpn. J. Appl. Phys.*, 1995, **34**, 4143.
13 (*a*) W. Kuhn, A. Naumov, H. Stanzl, S. Bauer, K. Wolf, H. P. Wagner, W. Gebhardt, U. W. Pohl, A. Krost, W. Richter, U. Dumichen and K. H. Thiele, *J. Cryst. Growth*, 1992, **123**, 605.
14 (*a*) D. N. Armitage, H. M. Yates, J. O. Williams, D. J. Cole-Hamilton and I. L. J. Patterson, *Adv. Mater. Opt. Electron.*, 1992, **1**, 43; (*b*) D. F. Foster, I. L. J. Patterson, L. D. James, D. J. Cole-Hamilton, D. N. Armitage, H. M. Yates, A. C. Wright and J. O. Williams, *Adv. Mater. Opt. Electron.*, 1994, **3**, 163.
15 K. Nishimura, K. Sakai, Y. Nagao and T. Ezaki, *J. Cryst. Growth*, 1992, **117**, 119.
16 K. Nishimura, Y. Nagao and K. Sakai, *J. Cryst. Growth*, 1993, **134**, 293.
17 N. Lovergine, M. Longo, C. Gerardi, D. Manno, A. M. Mancini and L. Vasanelli, *J. Cryst. Growth*, 1995, **156**, 45.
18 (*a*) P. O'Brien and R. Nomura, *J. Mater. Chem.*, 1995, **5**, 1761; (*b*) P. O'Brien, *Precursors for Electronic Materials*, in *Inorganic Materials*, ed. D. W. Bruce and D. O'Hare, John Wiley, London, 1992, p. 499; (*c*) M. Bochmann, *Chem. Vap. Deposition*, 1996, **2**, 85.
19 D. F. Foster and D. J. Cole-Hamilton, *Inorg. Synth.*, 1997, **31**, 29.
20 G. E. Coates and D. Ridley, *J. Chem. Soc.*, 1965, 1870.
21 G. E. Coates and A. Lauder, *J. Chem. Soc. A*, 1966, 264.
22 J. D. Kennedy and W. McFarlane, *J. Chem. Soc., Perkin Trans. 2*, 1977, 1187.
23 (*a*) M. Bochmann, K. J. Webb, M. Harman and M. B. Hursthouse, *Angew. Chem., Int. Ed. Engl.*, 1990, **29**, 638; (*b*) M. Bochmann, K. J. Webb, J. E. Hails and D. Wolverson, *Eur. J. Solid State Inorg. Chem.*, 1992, **29**, 155; (*c*) G. Kraüter and W. S. Rees, Jr., *J. Mater. Chem.*, 1995, **5**, 1265; (*d*) M. Bochmann, A. P. Coleman and A. K. Powell, *Polyhedron*, 1992, **11**, 507; (*e*) J. G. Brennan, T. Siegrist, P. J. Carroll, S. M. Stuczynski, L. E. Brus and M. L. Steigerwald, *J. Am. Chem. Soc.*, 1989, **111**, 4141; (*f*) W. S. Rees, Jr. and G. Kraüter, *J. Mater. Res.*, 1996, **11**,

3005; (*g*) R. D. Schluter, G. Kraüter and W. S. Rees, Jr., *J. Cluster Sci.*, 1997, **8**, 123; (*h*) M. L. Steigerwald and C. R. Sprinkle, *J. Am. Chem. Soc*., 1987, **109**, 7200; (*i*) J. G. Brennan, T. Siegrist, P. J. Carroll, S. M. Stuczynski, P. Reynders, L. E. Brus and M. L. Steigerwald, *Chem. Mater.*, 1990, **2**, 403.
24 N. L. Pickett, D. F. Foster, D. Ellis and D. J. Cole-Hamilton, *J. Mater. Chem.*, to be submitted.
25 S. W. Haggata, X. Li, D. J. Cole-Hamiltion and J. R. Fryer, *J. Mater. Chem.*, 1996, **6**, 1771.
26 M. G. Bawendi, A. R. Kortan, M. L. Steigerwald and L. E. Brus, *J. Chem. Phys.*, 1989, **91**, 7282.

Paper 8/06421K